Comparison of TRMM precipitation radar and microwave imager rainfall retrievals in tropical cyclone inner cores and rainbands

Joseph P. Zagrodnik[1] and Haiyan Jiang[1]

Received 11 April 2012; revised 4 November 2012; accepted 7 November 2012; Published 16 January 2013.

[1] Tropical Rainfall Measuring Mission (TRMM) rainfall retrieval algorithms are evaluated in tropical cyclone (TC) inner cores (IC), inner bands (IB), and outer rainbands (OB). In total, 1329 IC, 2149 IB, and 4627 OB storm regions are analyzed using data from a 12-year TRMM Tropical Cyclone Precipitation Feature (TCPF) database containing 1013 TCs viewed from December 1997 to December 2009. Attention is focused on the difference between the Precipitation Radar (PR) 2A25 and the TRMM Microwave Imager (TMI) 2A12 rainfall algorithms. The PR 2A25 produces larger mean rain rates than the TMI 2A12 in inner cores and inner bands, with the greatest difference occurring in hurricanes. This discrepancy is caused mostly by the TMI 2A12 significantly underestimating regions of moderate to heavy rain $>15\,\mathrm{mm\,hour^{-1}}$ or when the PR reflectivity is greater than 30 dBZ. The TMI 2A12 rain rates are most closely related to the percentage coverage of 85 GHz polarization-corrected brightness temperature (PCT) <225 K in the IC and 85 GHz PCT <250 K in the IB and OB. These convective parameters are good predictors of the mean TMI 2A12 rain rate, but significant ice scattering is not always present in areas of heavy rain that are often widespread in TC inner regions. As a result, the TMI 2A12 algorithm may poorly measure the rain rate, particularly in the inner core of hurricanes.

Citation: Zagrodnik, J. P., and H. Jiang (2013), Comparison of TRMM precipitation radar and microwave imager rainfall retrievals in tropical cyclone inner cores and rainbands, *J. Geophys. Res. Atmos.*, *118*, 29–42, doi:10.1029/2012JD017919.

1. Introduction

[2] Satellite precipitation retrievals are one of the best ways to observe the spatial distribution of precipitation in tropical cyclones (TCs) over ocean. Rainfall observations from the Tropical Rainfall Measuring Mission (TRMM) satellite have helped to quantify the total precipitation in tropical systems, initialize and validate numerical models, and decipher the relationship between TC eyewall and rainband structure and intensity changes. However, these algorithms are calibrated on a global or regional scale and often show less agreement for smaller scale features such as TCs. The rainfall retrievals must be derived using a number of assumed parameters related to the microphysical properties of cloud, rain, and ice particles. Numerous studies have compared the TRMM rain retrieval algorithms for a wide variety of applications. Focus is usually on regional or temporal biases caused by empirical assumptions of cloud microphysical parameters [e.g., *Berg et al.*, 2002, 2006; *Nesbitt et al.*, 2004]. Tropical cyclones present a unique challenge because they are especially sensitive to environmental parameters such as storm motion, wind shear, and moisture distribution, all of which can affect the vertical profile of cloud water and ice. The relationship between vertical cloud profiles and near-surface rainfall can be different in the inner and outer regions of TCs and in TCs compared with the ambient environment. The spatial distribution of precipitation in TCs is influenced by a number of dynamic and environmental factors that govern their convective structure. Weaker TCs and outer bands often produce light and sporadic rainfall, whereas inner regions of intense TCs are more likely to be proficient heavy rain producers.

[3] The TRMM Microwave Imager (TMI) and Precipitation Radar (PR) provide independent and complimentary estimates of near-surface rainfall. The TMI [*Kummerow et al.*, 1998] is a passive, multichannel microwave radiometer with an 878 km swath width (760 km before 2001 orbital boost). The TMI 2A12 rainfall algorithm [*Kummerow et al.*, 1996, 2001] retrieves surface rainfall from the full spectrum of TMI frequencies (10, 19, 21, 37, and 85 GHz). The algorithm is based on the Goddard Profiling algorithm and uses a Bayesian approach, with several cloud model integrations used to pair surface rain rates with the corresponding set of upwelling microwave brightness temperatures. In contrast, the Precipitation Radar (PR) has a narrower 247-km swath width (215 km before boost). The PR 2A25 algorithm [*Iguchi et al.*, 2000] retrieves rain rates from observed radar

[1]Department of Earth and Environment, Florida International University, Miami, Florida, USA.

Corresponding author: H. Jiang, Department of Earth and Environment, Florida International University, 11200 SW 8th St, PC-342B, Miami, FL 33199, USA. (haiyan.jiang@fiu.edu)

2169-897X/12/2013JD017919

reflectivities using a $Z-R$ relationship. The underlying physics are more straightforward for the PR 2A25 algorithm than for the TMI 2A12 algorithm, but still the PR 2A25 has to assume a particle size distribution model to derive rain rate from radar reflectivity. The most difficult part of the K-band TRMM radar rainfall retrieval is determining the beam attenuation, which increases with higher rain rates. The PR is generally considered to be accurate relative to ground data, but a few areas of greater uncertainty must be taken into consideration. *Wolff and Fisher* [2008] noted that PR 2A25 version 6 underestimates heavy rain rates relative to TRMM Ground Validation (GV) radar data over ocean. *Schumacher and Houze* [2000] compared the PR with the S-band Kwajalein oceanic validation radar and found that the PR's 17 dBZ minimum reflectivity threshold limits its ability to detect rain rates below $0.2-0.4\,\mathrm{mm\,hour^{-1}}$.

[4] The TMI 2A12 algorithm has been most commonly used in previous TRMM TC rainfall studies, because its wide swath accrues more observations. *Lonfat et al*. [2004] found that the TMI 2A12 (version 5) azimuthally averaged rain rates vary by both storm intensity and basin, with the greatest differences occurring in the innermost 100 km of the storm. With the same data set, *Chen et al*. [2006] added a shear-relative coordinate system to conclude that TC rainfall asymmetries depend on the juxtaposition and relative magnitude of the storm motion and vertical wind shear vectors. *Cecil* [2007] also used the TMI 2A12 to show that inner core rainfall in highly sheared Atlantic hurricanes is favored in the downshear – left quadrant, with mean rain rates of about $15-16\,\mathrm{mm\,hour^{-1}}$ compared with $6-7\,\mathrm{mm\,hour^{-1}}$ in the nonfavored quadrants. The TMI 2A12 is most directly compared with the PR 2A25 by *Cecil and Wingo* [2009]. They resized the pixels to a $0.25^\circ \times 0.25^\circ$ grid and directly compared the new grid boxes in TCs of various intensities. The two algorithms were found to agree closely on mean rain rates except in the innermost 100 km of hurricanes, where the PR 2A25 rain rates are greater than the TMI 2A12 by 2.9 mm $\mathrm{hour^{-1}}$ (9.5 vs. $6.6\,\mathrm{mm\,hour^{-1}}$). Another important finding was that the PR 2A25 contributes more rain to the mean from high rain rates, whereas the TMI 2A12 contributes more from light and moderate rain rates. When directly comparing the grid boxes, low PR 2A25 rain rates were most closely matched with low to moderate values for the TMI 2A12, and the highest PR 2A25 rain rates matched with only $10-15\,\mathrm{mm\,hour^{-1}}$ rain rates for the TMI 2A12. The linear correlation between the algorithms (for hurricane inner cores) is only 0.61 at the 0.25° grid size [*Cecil and Wingo*, 2009].

[5] The high-frequency, high-resolution TMI channels (85 and 37 GHz) are of utmost interest in understanding the TMI 2A12 algorithm. Lower frequency emission-based channels (10 and 19 GHz) are more sensitive to near-surface rain, but their influence on the TMI 2A12 algorithm in TCs is limited by their low resolution [*Shige et al*., 2006]. In particular, the beam-filling effect causes underestimation in situations in which small areas of heavy rain are embedded within a large footprint [*Wolff and Fisher*, 2008]. The 85 and 37 GHz polarization-corrected brightness temperatures (PCTs) are commonly used as proxies for rainfall and convective intensity in TCs [*Spencer et al*., 1989]. The 85 GHz PCT senses precipitation-sized frozen hydrometeors, with a lower PCT corresponding to more ice scattering and stronger convection. An 85 GHz PCT around 275 K indicates the presence of frozen hydrometers. An 85 GHz PCT below 250 K is an indicator of a light-to-moderate rain rate of at least $3\,\mathrm{mm\,hour^{-1}}$. When the 85 GHz PCT is lower than 225 K, the rain is considered to be convective with a rate of at least $10-12\,\mathrm{mm\,hour^{-1}}$ [*Mohr and Zipser*, 1996]. Intense convection is present when the 85 GHz PCT drops below 200 K. The 37 GHz PCT is sensitive to larger ice hydrometers. The 37 GHz PCT has a smaller dynamic range than the 85 GHz PCT and varies only from about 280 to 250 K in most cases [*Cecil et al.*, 2002], although it is capable of dropping below 200 K in stronger convection. In practice, the relationship between ice scattering and surface rainfall is complicated. It is generally accepted that PCT criteria can be equated with near-surface rain rates in the terms described above, but in many cases the rain rates can vary drastically for similar PCT criteria. The exact value depends on several interconnected factors, including the stage of the convective system (i.e., developing, mature, or dissipating). Furthermore, various geographic and environmental factors, such as vertical wind shear and the presence of dry air, can alter the microphysical properties of cloud liquid and ice and hence the precipitation retrievals.

[6] The main goal of this study is to compare the properties of the TRMM PR 2A25 and TMI 2A12 rainfall retrieval algorithms in TC inner cores and rainbands. The methodology does not involve a pixel-by-pixel comparison but rather involves an evaluation of the rainfall distributions in the storm regions (inner cores, inner rainbands, outer rainbands) as a whole. However, to make a fair comparison, a nearest-neighborhood method is used to average PR 2A25 resolution to TMI 2A12 resolution (see section 2 for details). In the first part of this study (see section 3), algorithm rain estimates are stratified by storm region and TC intensity and compared in three ways: mean values, histograms, and scatterplots. From this analysis, it becomes clear that there is a significant difference in the two algorithms in TCs, especially for the inner cores of intense storms. The second half of this study (section 4) looks at the relationship between 37 and 85 GHz convective parameters and the rain rate retrievals. The properties of moderate and heavy rain are emphasized, because the highest rain rates contribute the most to the mean. The key issues in understanding why the algorithms disagree in TCs are: 1) how the TMI estimates heavy rain through the 37 and 85 GHz scattering channels and 2) how the estimates of the moderate and heavy rain rates compare between the PR and the TMI. Understanding the characteristics of these retrievals is important for accurately interpreting TC precipitation and improving future versions of satellite precipitation algorithms. Tropical cyclones offer some of the best extreme rain data, because heavy rain rates that are generally rare in the tropics are often widespread in TCs. This study focuses specifically on TRMM, but the broader conclusions are applicable to a wide range of satellite-based tropical precipitation studies in which accurate estimation of moderate and heavy rain rates influences the results.

2. Data and Methods

[7] This study utilizes the TRMM Tropical Cyclone Precipitation Feature (TCPF) database [*Jiang et al*., 2011] to compare rainfall retrievals in TCs. The TCPF database is a subset of the University of Utah (UU) TRMM Precipitation

Table 1. Mean, Minimum, Maximum, and Standard Deviation of the Outer Edge of Storm Region Separation Radii

Region	Mean Radius (km)	Min Radius (km)	Max Radius (km)	Std. Deviation
IC	87	45	170	18
IB	164	90	270	28
OB	505	300	900	123

Feature (PF) database [*Liu et al*., 2008]. The TCPF database includes global TC best-track information, collocated PR and TMI measurments and retrievals, and environmental parameters derived from NCEP realanysis. The time frame spans 12 years from December 1997 to December 2009, consisting of 13,677 individual TRMM overpasses of 1013 TCs. Two rainfall algorithms are compared: the Precipitation Radar 2A25 algorithm (PR 2A25) version 6 and the TRMM Microwave Imager 2A12 algorithm (TMI 2A12) version 6. The PR 2A25 product has a pixel size of 5×5 km (4×4 km before boost) compared with 8×6 km (7×5 km before boost) for the TMI 2A12 retrieval. Because of the resolution difference between the retrievals, the pixels cannot be directly compared. This study uses a nearest-neighbor method similar to that of *Nesbitt et al*. [2000] to average PR pixels to the TMI 2A12 product resolution. One note here is that the 2A12 orbital product has retrieval estimates at every 85 GHz field of view (FOV), whereas the actual resolution of the TMI retrieval estimate is complicated because the algorithm uses 10-, 19-, 37-, and 85 GHz channels, which have different FOVs. Here our comparison is based on the perspective of end users of the algorithm instead of an algorithm developer. Therefore, the PR resolution is downgraded only to the resolution of the TMI 85 GHz FOV and not any further.

[8] To compare the TC rainfall, the TCPFs are subjectively subclassified into three subregions for detailed study. The motivation for the orbit divisions has been described by *Cecil et al*. [2002], and the manual division of subregions was performed by *Jiang et al*. [2012] for the 12-year TCPF database. Further details and an example have been detailed by *Jiang et al*. [2012]. The inner core (IC) region includes the eyewall and all near-center convection in storms without eyewalls. The inner rainband (IB) region includes banded or blob-like precipitation immediately outside the area of strongest 85 GHz ice scattering associated with the IC. A rain-free region approximately 150−200 km from the center usually separates the IB from the outer rainband (OB), which includes outward-spiraling rainbands and all outlying TC-related features. Each storm is assigned IC, IB, and OB radii, which represent the outer edges of these storm regions. Compared with a fixed 100-km radius, the subjective method accounts for varying TC size and reduces the contamination between the IC and IB regions. Minor contamination still occurs in weak TCs and TCs in which the boundaries between the regions are not easily distinguishable. The regions are always circular, so highly asymmetric TCs also exhibit some contamination. Storms are also divided into four intensity categories, as follows. Tropical depressions (TDs) have maximum sustained winds of 34 knots or less; tropical storms (TSs) have winds from 35 to 63 knots, category 1/2 hurricanes (cat. 1/2) have winds from 64 to 95 knots; and category 3−5 hurricanes (cat. 3−5) have winds of 96 knots or greater.

[9] To generate the data set, all PR pixels within one TMI FOV are averaged to the TMI resolution. The TMI pixels and the corresponding PR pixels are then grouped into the IC, IB, and OB regions. Only nonzero pixels are included, meaning that all rainfall statistics in this study are conditional rain rates. One exception is for zero-rain PR pixels that are collocated to the same TMI pixel as a nonzero PR 2A25. In this way, both algorithms are compared at the lower resolution of the TMI 2A12 retrieval. The PR and TMI pixels for each storm are different in number, size, and coverage area depending on where each algorithm detects rain. To make a direct comparison, the saved PR and TMI raining pixels from each storm and region (IC, IB, and OB) are integrated to form a single feature for the IC, IB, and OB region of each storm. For a sample to be accepted, the TC center and all individual raining pixels must be centered over the ocean. Up to five pixels over a very small landmass such as an island are still accepted as being over ocean.

[10] The regions are considered independently so that an IC can still be accepted even if some of the rainbands from the storm are located over land. To remove samples that capture only a small portion of the storm region, minimum PR 2A25 raining area criteria of 5000 km^2 are also set for each individual region. The size criteria ensure that storm regions have approximate swath coverage (based on visual approximation) of at least 60% in the IC, 40% in the IB, and 20% in the OB. The mean swath coverage relative to the circular or annular storm region after applying the criteria is 79% in the IC, 56% in the IB, and 26% in the OB. Table 1 displays the characteristics of the storm region separation radii. The mean IC radius is 13% (12 km) smaller in cat. 3−5 hurricanes than in TDs. The IB and OB radii do not change significantly with intensity. The TC center locations of the final sample are displayed in Figure 1, with the sample size in parentheses. In total, 1329 IC, 2149 IB, and 4627 OB regions are considered. Because of the relatively small size of the IC and IB regions relative to the OB, the PR swath often misses the inner regions entirely.

[11] A number of storm parameters from the TCPF database are calculated for each storm region. Storm parameters such as center location and intensity are derived from best-track data, which are obtained from the National Hurricane Center (NHC) for the Atlantic and eastern North Pacific basins and from the Joint Typhoon Warning Center (JTWC) for all other basins. Two raining parameters are derived directly from satellite data: raining area (km^2) and rain rate (mm $hour^{-1}$), both of which are calculated separately for the PR and TMI. These two parameters can be multiplied to measure the volumetric rainfall (mm $hour^{-1}$ km^2), which is defined as the rain flux (rain rate multiplied by raining area) at the instantaneous time of the overpass. Convective parameters include the TMI 37 and 85 GHz PCT (K) and the PR reflectivity (dBZ). Traditionally, the minimum PCT value and maximum 20 dBZ echo height (km) are used to represent the strongest point of convection within a designated TC region. In this study, emphasis is placed on the aerial coverage of the PCT and near-surface PR reflectivity by calculating the percentage of coverage of these convective parameters in each storm region relative to the total raining area. This method was also employed by *Cecil and Zipser*

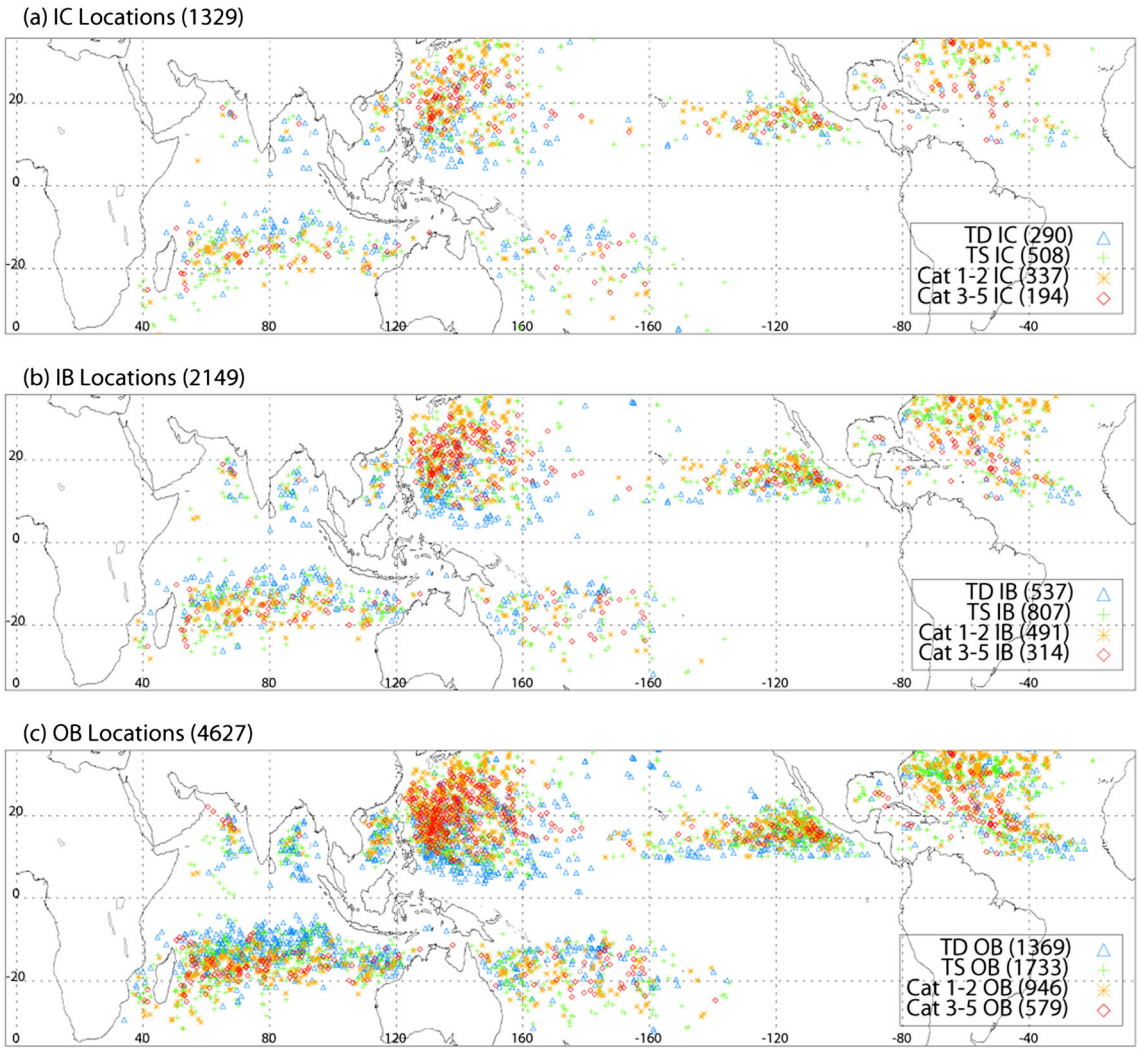

Figure 1. TC Center locations of storms with accepted IC (a), IB (b), and OB (c) features with a PR 2A25 raining area >5,000 km^2. Numbers in parentheses indicate the total sample size.

[1999] and is a convenient way to measure the fraction of raining area that meets various convective criteria. Specific criteria for the TMI (calculated relative to TMI 2A12 raining area) include the percentage of 37 GHz PCT less than 250 and 225 K and 85 GHz PCT less than 275, 250, 225, 200, and 175 K. The percentage of 20, 30, and 40 dBZ near-surface reflectivity (relative to PR 2A25 raining area) is also calculated. The percentage coverage criteria are more closely related to TC rainfall than the minimum PCT criteria, because they consider the convective properties over a larger area instead of just an individual point.

3. Statistical Comparison of Rainfall Algorithms

3.1. Mean Rainfall Values

[12] Mean values (per storm region) are calculated to account for differences in sample sizes between the storm regions and intensities. Figure 2 displays the mean values for raining area, rain rate, and volumetric rain for storm regions of various intensities. Because each TRMM overpass covers a different fraction of the storm, the absolute raining area and volumetric rain values are not significant, only the relative difference between algorithms. In Figure 2a and 2b, the raining area for PR 2A25 is shown to be less than the raining area for TMI 2A12 in all regions and intensities. The mean raining area (km^2) is the average area in each storm region where rainfall is nonzero. The difference between the algorithms is about the same across the board, with the TMI 2A12 producing a 10−20% larger raining area. More intense storms show an overall larger raining area in the IB and OB. The raining area also increases with intensity in the IC, but the trend is offset with this analysis method because the mean IC radius in hurricanes is about 10 km less than the radius in tropical depressions and storms.

[13] Several factors cause the TMI 2A12 raining area to be larger than the PR 2A25. One issue is the TMI's lower resolution, which slightly overestimates the size of almost all raining features. Larger differences are observed in light-banded rain features. In a typical light rainband, the PR 2A25 detects numerous small showers, whereas the TMI 2A12 identifies a single large PF, which in some instances can be five times or more than the sum of the individual 2A25 PFs. In many of these cases, the low-frequency (10,

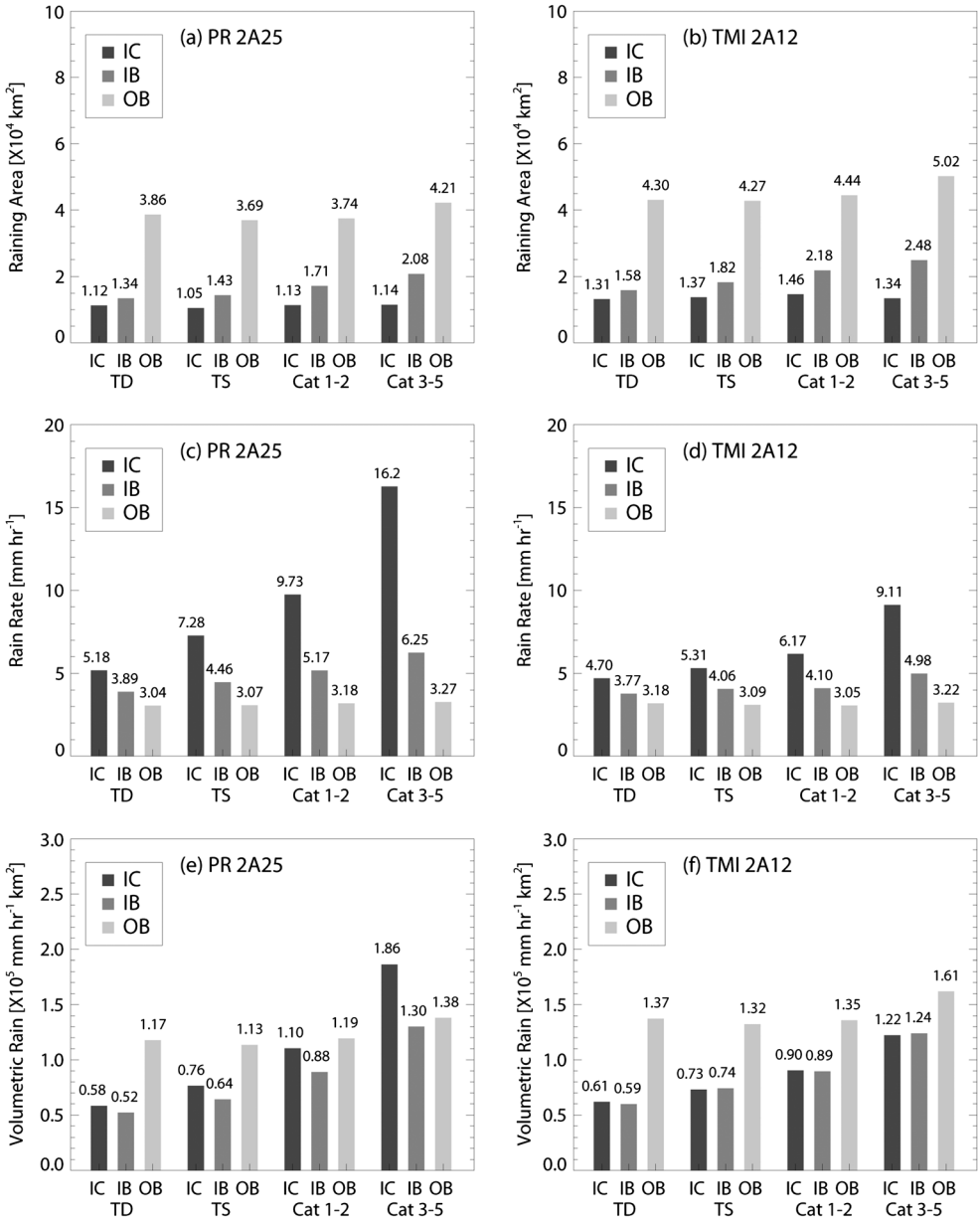

Figure 2. Bar plots comparing PR 2A25 and TMI 2A12 mean raining area (a,b), mean rain rate (c,d), and mean volumetric rain (e,f) for inner cores (dark shade), inner bands (medium shade), and outer bands (light shade), divided by storm intensity.

19 GHz) TMI channels may have difficulties distinguishing between elevated cloud liquid water levels and light precipitation. It is also difficult for the algorithm to resolve small-scale, warm-rain features while incorporating the low-resolution 10 and 19 GHz channels. Additionally, the PR may be missing very light drizzle (rain rate <0.3 mm hour^{-1}) because of its 17−18 dBZ minimum reflectivity threshold [*Schumacher and Houze*, 2000; *Berg et al*., 2006]. Independent ground validation data are required to decide whether it is raining or not in these situations. The TMI 2A12 raining area is also larger than PR 2A25 in areas of deeper convection. The ice-scattering signature of heavier precipitation can extend beyond the region of surface precipitation, such as into the rain-free eye of major hurricanes or downshear of a region of deep convection [*Cecil et al*., 2002].

[14] The mean conditional rain rates are compared in Figure 2c and 2d. The PR 2A25 produces larger rain rates than the TMI 2A12 in the IC and IB, with the difference always increasing with greater storm intensity. In the OB region, both algorithms show similar mean rain rates between 3.0 and 3.3 mm hour^{-1} for all intensities. The difference between PR 2A25 and TMI 2A12 is greatest in the IC, especially hurricanes, for which the mean PR 2A25 rain rate is over 50% higher than the TMI 2A12. In absolute terms, the PR 2A25 is greater by only 0.5 mm hour^{-1} in TD inner cores, but it rises to 1.0 mm hour^{-1} in TSs and 3.6 and 7.1 mm hour^{-1} in cat. 1/2 hurricanes and in major hurricanes. A modest difference is observed in the IB, ranging from 0.1 mm hour^{-1} in TDs up to 1.3 mm hour^{-1} in major hurricanes. Compared with rain rates of *Cecil and Wingo* [2009; Figure 2], the rain rates for

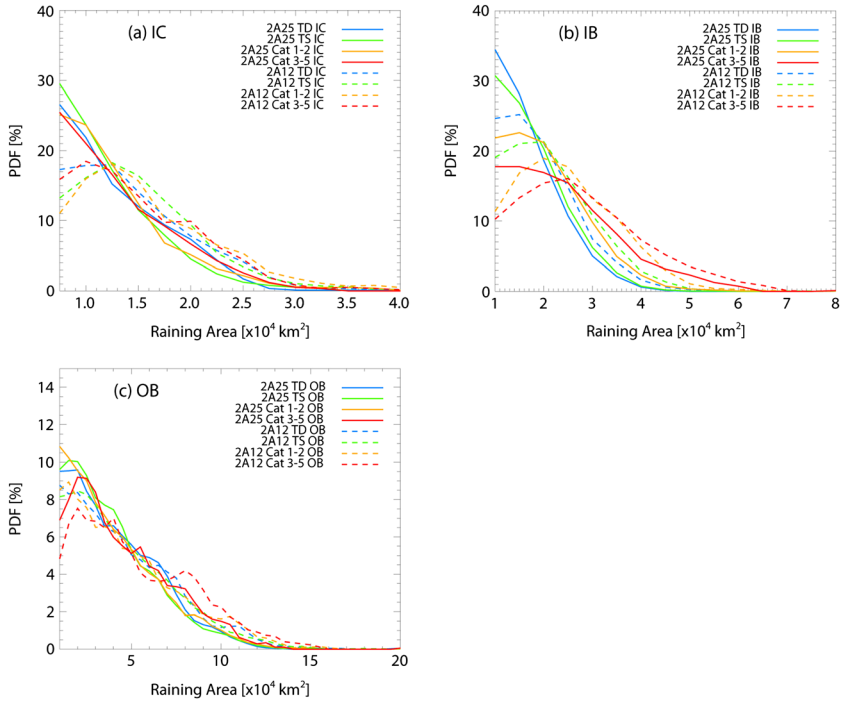

Figure 3. PDF of raining area distributions for IC (a), IB (b), and OB (c) regions, divided by algorithm and intensity.

both algorithms in this study are significantly larger in all instances, from a factor of about one third in hurricane inner cores (0–100 km) up to a factor of 4−6 in both weaker storms and in the OB (200−500 km). *Cecil and Wingo* [2009] found close agreement between the algorithms everywhere except for hurricane inner cores. The discrepancy between the studies is likely caused by *Cecil and Wingo* [2009] resizing the PR and TMI pixels to a 0.25° grid. The large grid size lowers the mean rain rate by including nonraining pixels that are adjacent to raining pixels into the grid. The primary area of interest is the inner core, where the difference in rain rates cannot be explained by differences in instrument or sample resolution.

[15] Figure 2e and 2f displays the mean volumetric rain in the same manner. Volumetric rain is a useful comparison tool in that it normalizes the difference in raining area between the two algorithms. Both algorithms again show the same general trends, with stronger intensity corresponding to more volumetric rainfall. The outer bands vary the least between intensity categories, and all have about 15% more TMI 2A12 volumetric rain. The inner bands actually show better agreement than the outer bands between the two algorithms. The most significant difference is again in the inner core of hurricanes, where the PR 2A25 is close to the TMI 2A12 in weaker storms but larger by up to about 50% in the cat. 3−5 range. In considering the raining area, rain rate, and volumetric rain as a whole, several areas of interest emerge. In the outer bands, the higher TMI 2A12 volumetric rain totals can be explained almost completely by higher TMI 2A12 raining areas, because the OB rain rates agree closely. In the inner regions, especially hurricane inner cores, higher PR 2A25 rain rates offset the larger TMI 2A12 raining areas, resulting in greater PR 2A25 volumetric rain totals relative to the TMI 2A12. In the outer regions and in weak storms, a large part of the inconsistency comes from differences in rain detection, as reflected in the differences in raining area. In strong storms with greater rain coverage, the actual rainfall intensity becomes the dominant source of disagreement.

3.2. Rainfall Distributions

[16] To analyze further the source of the algorithm disagreement, the three PDFs are shown in Figure 3 for raining area in the IC, IB, and OB (Figure 3a–3c, respectively). The PR 2A25 estimates smaller raining areas in the IB and OB, but the raining areas for stronger storms have a broader distribution. More intense storms tend to have larger raining areas, almost entirely because of the expansion of the rain field in the geographically larger IB and OB regions. The TD and TS curves are also closely grouped for the TMI, but there is some separation, especially in the IB. In the IC, storm intensity has almost no influence on raining area, except for a small increase in larger raining areas for PR 2A25 hurricanes. The distributions are grouped closely by algorithm, with the PR 2A25 finding much smaller raining areas compared with the TMI 2A12.

[17] The PDFs for rain rate are displayed in Figure 4. In the IC, the distributions show high variability between algorithms and intensity categories. The algorithms are in best agreement for TDs and farthest apart for major hurricanes. All intensity categories follow the same pattern. The TMI 2A12 distributions are closer to a Gaussian distribution and have lower modes than the PR 2A25. The PR 2A25 has broader distributions that become positively skewed and have higher modes for stronger intensity categories. The histograms for hurricanes are of most interest because of the significant disagreement between algorithms. The TMI 2A12 has only seven cases with a rain rate greater than 15 mm hour^{-1}, whereas the PR 2A25 detects 103 ICs with rain rates in the 15–40 mm hour^{-1} range. These totals

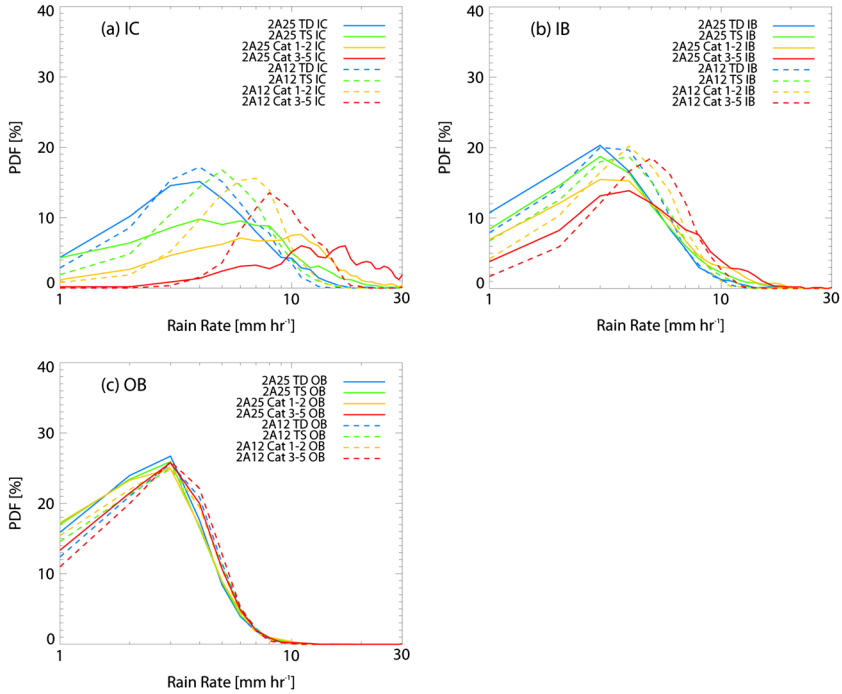

Figure 4. PDF of rain rate distributions for IC (a), IB (b), and OB (c) regions, divided by algorithm and intensity.

represent 53% of the PR 2A25 and just 4% of the TMI 2A12 cat. 3−5 inner cores. For cat. 1/2 hurricanes, the PR 2A25 finds 16% of cases with a rain rate greater than 15 mm hour^{-1} and not a single case for the TMI 2A12. The TMI 2A12 places the majority of hurricane ICs in the 5−15 mm hour^{-1} range.

[18] There are significant differences between this IC region-based distribution and the grid-based distribution in *Cecil and Wingo* [2009]. For the 0.25° grid scale, the 0−100 km PR 2A25 rain rate mode is always the >0−1 mm hour^{-1} bin for all intensities. Despite the abundance of low PR 2A25 rain rates, they found that about two thirds of the mean cat. 3−5 rain rate is derived from grids with rain rates greater than 15 mm hour^{-1}. In weaker storms, the PR 2A25 has a smaller fraction of heavy rain grids (>15 mm hour^{-1}) and more very light rain grids (<3 mm hour^{-1}). Therefore, the IC region histograms in Figure 4a peak in the midrange, because the relatively small sections of heavy PR 2A25 rain rates skew the histograms toward 5−15 mm hour^{-1} rain rates, even though on a smaller grid or pixel level these rain rates are less common. For the TMI 2A12, the 0.25° grid-based rain rate histograms also show two separate peaks in hurricanes, but the higher peak is in the 5−15 mm hour^{-1} range. The region-based analysis is in fairly close agreement with the grid-based analysis for the TMI 2A12 except that the peak at low rain rates (<2 mm hour^{-1}) does not appear in this study because the low rain rates contribute only a small portion of the total rain rate and are averaged out when we compute for the entire inner core.

[19] Inner bands also exhibit broader PR 2A25 distributions compared with the TMI 2A12, inasmuch as the IB is still skewed slightly toward higher PR 2A25 and TMI 2A12 rain rates. There is not as much of a spread between different intensities in the IB, but values of 10−20 mm hour^{-1} rain rates are still largely absent from the TMI 2A12. In the OB, the standard deviation is the lowest, and there is almost no difference between the algorithms. The mode is always the 2−3 mm hour^{-1} bin in the OB and does not increase with intensity as in the IC and IB. Overall, the storm-based PDFs are good compliments to the grid-based PDFs from *Cecil and Wingo* [2009]. The grid-based PDFs show that each algorithm derives its mean rain rates from a different set of rain rates. The storm region-based PDFs show that each intensity category also consists of a climatologically wide range of mean rain rates, especially in the inner regions. The PR 2A25 suggests that an individual hurricane has a wider range of possible mean rain rates than what would be expected from the TMI 2A12.

[20] Volumetric rain distributions are displayed in Figure 5. In the IC, the spread is about the same in storms of TD and TS intensity, with good agreement between the algorithms. The only major difference is found in cat 3−5 hurricanes, which are skewed toward higher rain totals. The separation between the algorithms in hurricanes is caused by the long tail of PR 2A25 inner cores with volumetric rain greater than 4×10^4 mm hour^{-1} km^{-2}. A similar pattern is observed in the inner bands, except with higher mean values and a larger spread between the intensity categories. The best agreement between the algorithms is found in the OB. The 2A25 does find more storms with small amounts of rain, but the distributions are nearly equal in storms with more rain. Increased intensity produces almost no increase in OB volumetric rain.

3.3. Algorithm Correlations

[21] Scatterplots of the volumetric rain, rain area, and rain rate (Figure 6) are useful for comparing the algorithms on a

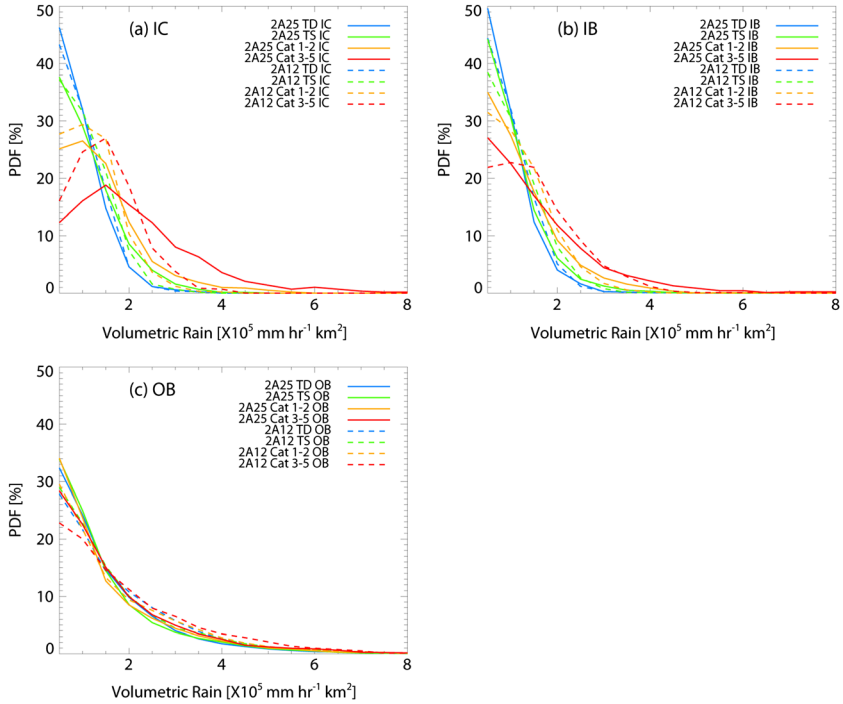

Figure 5. PDF of volumetric rain distributions for IC (a), IB (b), and OB (c) regions, divided by algorithm and intensity.

case-by-case basis. In Figure 6a–6c, the raining area is shown to be higher for the TMI 2A12 in almost every case for all three regions. The algorithms correlate well, with a fairly uniform bias toward the TMI 2A12. Regions with a smaller raining area still strongly favor the TMI 2A12, although there is a little more spread than for larger raining areas. It is possible for the PR 2A25 area to be larger than the TMI 2A12, especially in the OB, but this usually occurs only in small, isolated areas where the PR detects extremely light rain. The uniform nature of the TMI 2A12 bias suggests that the discrepancy between the raining areas is not related to the environmental conditions. Storm intensity and convective intensity (i.e., minimum 37 and 85 GHz PCT) do not affect the correlations in any significant way.

[22] The scatterplot for IC rain rate (Figure 6d) shows a strong bias toward higher PR 2A25 rain rates, especially for intense storms with heavy PR 2A25 rain rates. The majority of cat. 3−5 ICs have a higher PR 2A25 rain rate by a significant margin. In the most extreme cases, the IC rain rate is 20−30 mm hour^{-1} greater than the TMI 2A12. Still, many ICs, including some hurricanes, show very good agreement between the algorithms. In 58% of ICs, the algorithms are within 2 mm hour^{-1} of each other. For rain rates above 10 mm hour^{-1}, the PR 2A25 rain rate is almost always higher. If the rain rate is below 10 mm hour^{-1}, about one fourth of ICs have a higher TMI 2A12 rain rate. Most of the storms with lighter rain rates are below hurricane strength, so it is not surprising that the correlation coefficient is highest for weaker storms (≥0.75).

[23] In the IB, storms of different intensities are not as separated. Around one-half of IBs have a higher TMI 2A12 rain rate compared with the PR 2A25. As in the IC, the storms with higher PR 2A25 rain rate are still consistently biased toward the PR 2A25. Finally for the OB, the correlations are higher than in the IC or IB, but the scatterplot is shifted more consistently toward the PR 2A25 than in the other regions. Less than 10% of OBs have a higher TMI 2A12 rain rate. The more tightly clustered rain rates in the OB are likely caused by the lack of large regions of heavy precipitation in the outer regions of TCs. The PR 2A25 rain rate rarely exceeds 10−12 mm hour^{-1} in the OB. The grid-based scatterplot of *Cecil and Wingo* [2009] shows TMI 2A12 rain rates topping out at 10−15 mm hour^{-1} within 100 km of the TC center. Higher PR 2A25 rain rates are less common in the outer bands, even for hurricanes, so the differences between the algorithms are less substantial.

[24] Correlations are very high for volumetric rain, with values of about 0.80−0.90 in the IB and IC and over 0.90 in the OB. Storms in the IC are split almost exactly between having more PR 2A25 and more TMI 2A12 rain, with weak storms and lower volumetric rain values highly biased toward the TMI 2A12 and strong storms (especially cat. 3−5 hurricanes) and higher volumetric rain values biased toward the PR 2A25. In the IB, the trend is similar but shifted more toward the TMI 2A12. There is also less of an intensity bias, with the majority of storms clustered in the middle and not separated by intensity. The OB has virtually no separation by intensity categories, and the correlation coefficient is remarkably close to one, with almost no bias for high volumetric rain values. There is a slight bias toward the TMI 2A12, insofar as about 75% of outer bands have more TMI 2A12 rainfall. For the storms with the most volumetric rain, the bias still shifts slightly toward the PR 2A25. As a whole, the volumetric rain agrees best between the algorithms because of a higher TMI 2A12 raining area multiplied by higher PR 2A25 rain rates. Light rain rates favor

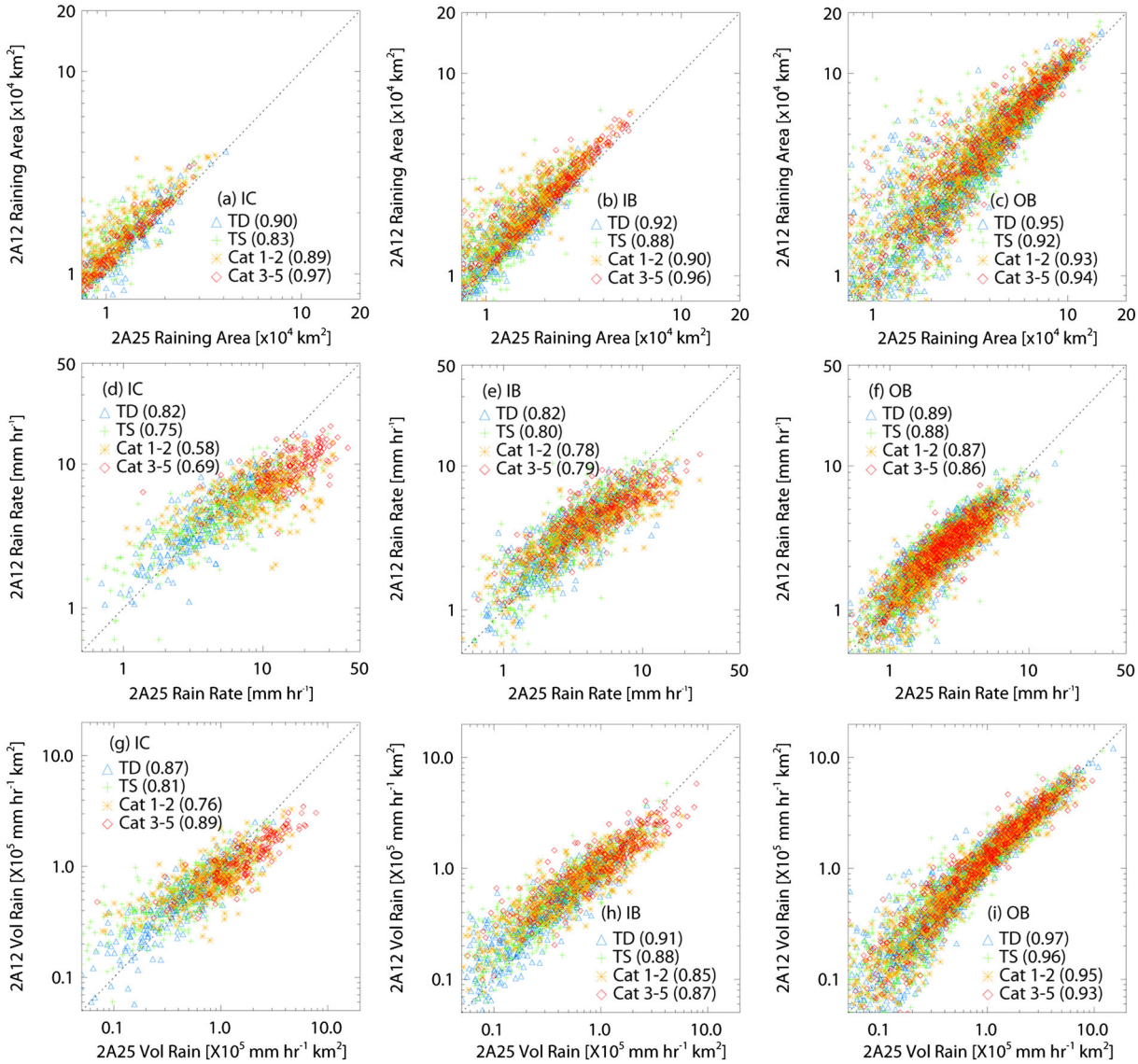

Figure 6. Scatterplots of PR 2A25 vs. TMI 2A12 raining area, rain rate, and volumetric rain, divided by IC, IB, and OB. Correlation coefficients are in parentheses for each intensity category.

more TMI 2A12 volumetric rain. Heavier rain rates favor more PR 2A25 volumetric rain.

4. Rain Rate in Relation to Convective Parameters

4.1. 85 and 37 GHz PCT

[25] The raining area, rain rate, and volumetric rain plots provide a comprehensive analysis of the differences in algorithm retrievals between TC regions with various intensities. The remainder of this article shifts focus to finding physical insights that can help to explain variations in the observed rainfall retrievals. For the PR, the relationship between rain rate and near-surface reflectivity is relatively straightforward. The percentage of raining area greater than 20, 30, and 40 dBZ quantifies the relative frequency of light, moderate, and heavy rain. The TMI 2A12 algorithm is less direct, in that it employs Bayesian probability to retrieve the rain rate from the full set of brightness temperatures at multiple TMI frequencies. Low-frequency emission-based channels (10.7, 19 GHz) are most sensitive to near-surface rainfall and are not saturated until high rain rates are reached, greater than 25 mm hour^{-1}. Unfortunately, the low-frequency channels have a much lower resolution than the TMI 2A12 pixel size, so they are not capable of resolving any finer-scale details of TC precipitation [*Kummerow et al.*, 1996]. Higher-frequency scattering-based channels (37, 85 GHz) have a better resolution but are sensitive mostly to ice scattering in the upper levels of the cloud. The 85 GHz frequency is the only channel with the same horizontal resolution as the TMI 2A12 algorithm, so its properties are of most interest to understanding the TMI 2A12 rain retrievals. The 85 and 37 GHz PCT are also commonly used as measures of convective intensity, because the PCT values can drop precipitously in deep convection with strong ice scattering.

Table 2. Percentage of Raining Pixels Meeting Various Convective Thresholds[a]

Region	Intensity	85 GHz PCT <275 K	85 GHz PCT <250 K	85 GHz PCT <225 K	85 GHz PCT <200 K	37 GHz PCT <275 K	37 GHz PCT <250 K	PR refl. >20 dBZ	PR refl. >30 dBZ	PR refl. >40 dBZ
IC	TD	70.4	30.7	11.7	4.9	43.6	1.6	48.5	24.2	4.2
	TS	68.3	31.5	12.8	5.4	47.7	1.8	50.4	27.7	5.9
	Cat. 1/2	76.9	36.4	12.7	4.1	59.4	1.2	52.5	33.2	8.3
	Cat. 3−5	85.8	52.1	20.6	6.2	73.1	2.1	57.0	41.3	12.2
IB	TD	63.2	23.0	6.7	2.3	35.3	0.8	42.4	18.6	2.3
	TS	62.4	24.2	7.7	2.2	42.3	0.8	44.1	21.0	2.7
	Cat. 1/2	70.2	26.2	5.6	1.1	53.5	0.5	46.5	23.6	3.1
	Cat. 3−5	79.2	30.9	5.7	1.0	59.7	0.6	47.6	25.7	3.1
OB	TD	52.0	15.6	4.4	1.7	25.2	0.7	35.4	13.4	1.4
	TS	50.8	15.4	4.2	1.5	29.0	0.6	35.3	13.7	1.4
	Cat. 1/2	51.1	15.5	3.3	1.0	33.3	0.5	35.2	13.7	1.4
	Cat. 3−5	55.3	16.6	3.1	0.9	35.2	0.3	35.4	13.8	1.3

[a]For 85 and 37 GHz PCT criteria, the percentage is calculated relative to TMI 2A12 raining pixels. For PR reflectivity criteria, the percentage is calculated relative to PR 2A25 raining pixels. All values are sorted by storm region and intensity.

[26] One convenient analytical method is to evaluate the mean distributions of various raining/convective parameters. Table 2 displays results for the percentage coverage 85 and 37 GHz PCT and 20, 30, and 40 dBZ reflectivity thresholds relative to raining area. All of the parameters have the highest percentage coverage in the IC and the lowest in the OB. The parameters that represent more intense convection (lower PCT, higher reflectivity) represent a smaller portion of each storm compared with the parameters representing light or moderate rain (higher PCT, lower reflectivity). In the IC, cat. 3−5 hurricanes have the highest percentage of all of the displayed parameters, but the difference is most significant for 85 GHz PCT (<250 and 225 K) and 37 GHz PCT (<275 K). This result is consistent with results from *Cecil and Zipser* [1999], who also found aerial coverage of 85 GHz PCT <250 K in the IC region to be correlated with stronger storm intensity. Notably, the IC coverage of 85 GHz PCT <250 K changes little between TDs, TSs, and cat 1/2 hurricanes. The IC coverage of 85 GHz PCT < 200 K actually has a slight decrease in cat. 1/2 hurricanes compared with TDs and TSs. Cat 3−5 hurricanes show a significant jump in 85 GHz PCT <250 K coverage, up over 15% from that of cat. 1/2 hurricanes. The same pattern is observed for 85 GHz PCT <225 K coverage, with a jump from 12.7% to 20.6% between hurricanes and major hurricanes. Parameters indicative of stronger ice scattering (85 GHz PCT <200 K, 37 GHz PCT <250 K) also show the same pattern in the IC. The lowest coverage occurs in cat. 1/2 hurricanes, and the highest coverage occurs in cat. 3−5 hurricanes. However, the coverage of deeper convection is relatively limited, averaging less than 6% of raining area at most. A sizeable portion of the ICs (about one fourth of TD, TS, and cat. 1/2 and 15% of cat. 3−5) have a minimum 85 GHz PCT above 200 K, indicating no deep convection at all. The 85 GHz PCT drops below 175 K in only about half of all ICs.

[27] The coverage of TMI convective parameters in the IB is similar to that in the IC, with a few notable exceptions. The percentages of coverage of 85 GHz PCT < 275 K and <250 K show modest increases for cat. 3−5 hurricanes, but the coverage of 85 GHz PCT <225 K is actually highest in weaker storms, in terms of both physical area (square kilometers) and percentage of raining area. The relative lack of convection in hurricane IBs was first observed using lightning data by *Molinari et al*. [1999] and was documented using a TRMM convective parameters similar to those of this study by *Jiang et al*. [2012]. The convective minimum in the IBs indicates that the ratio of stratiform rain to convective rain is higher in the IBs than in the inner core. In the OB, the convective parameters show little change between intensity categories. Only about one sixth of the OB raining area has an 85 GHz PCT below 250 K, and <5% of OB raining area meets the 85 GHz <225 K criteria for moderate rain. The percentage coverage by deep convection in the OB region is about the same as in the IB; the minimum 85 GHz PCT drops below 200 and 175 K in about the same fraction of OBs as IBs.

[28] All of the 85 and 37 GHz PCT coverage parameters can be compared with the TMI 2A12 rain rate for each storm. Only the higher PCT values can be correlated with rain rate, because the lower values (85 GHz PCT <200 K, 37 GHz PCT <250 K) have coverage too low to be significant. The two parameters with the best correlation are displayed in Figure 7, the coverage of 85 GHz PCT <250 K and <225 K. In the IC, the TMI 2A12 rain rate retrievals correlate well with the coverage of 85 GHz PCT <250 K and <225 K. In the IB and OB, the rain rate correlates best with the area of 85 GHz PCT <250 K. Weaker storms (TDs and TSs) tend to have a higher correlation than hurricanes. For 85 and 37 GHz PCT <275 K (not shown), the correlations between percentage of coverage and TMI 2A12 rain rate are still fairly high (0.4−0.7), but not as high as the scatterplots in Figure 7. In general, there is not much difference in scatter between storms of different intensities. In the IC, cat. 3−5 hurricanes tend to have higher rain rates and convective coverage, which clusters the points and lowers the correlation coefficient. Differences are more subtle in the OB. Cat 3−5 OBs actually show the opposite tendency and rarely have more than 20% coverage of 85 GHz PCT <225 K. The physical area of 85 GHz PCT <225 K does actually slightly expand in cat. 3−5 OBs relative to TD OBs, but the increase is offset by a larger increase in the raining area. The OBs consist of mostly warm PCTs (about 85% of raining area >250 K) and only isolated patches of ice scattering with little relation to storm intensity. Deep convection is localized and likely is not a strong contributor to the difference in PR 2A25 and TMI 2A12 rain rates. In the IB and OB, the deep convective bursts that trigger 85 GHz

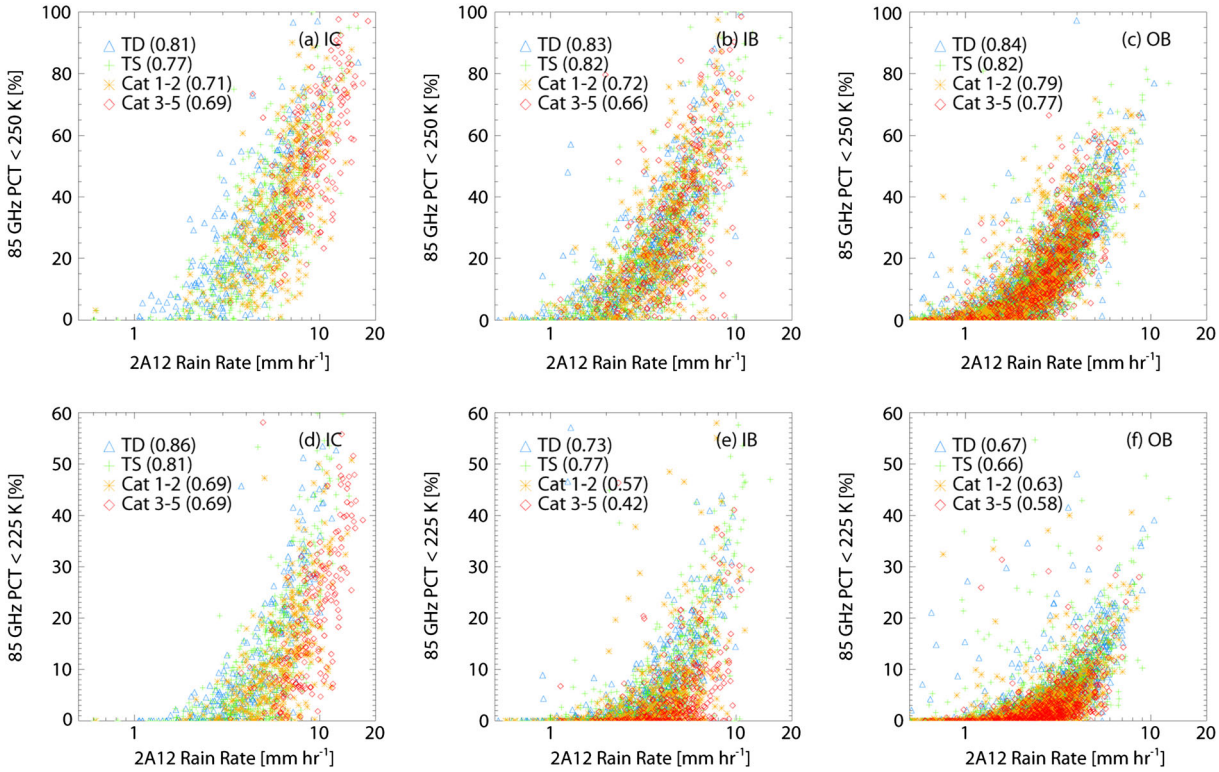

Figure 7. Scatterplots of TMI 2A12 rain rate vs. percentage coverage of 85 GHz PCT <250 and 225 K. Plots are divided by IC, IB, and OB storm regions.

PCT values below 200 K are no more widespread in intense hurricanes than they are in TDs or TSs.

4.2. 20, 30, and 40 dBZ PR Reflectivity

[29] From the TRMM Precipitation Radar, the percentage coverage of near-surface reflectivity greater than 20, 30, and 40 dBZ relative to PR 2A25 raining area is displayed in Table 2. As expected, the largest portions of high reflectivities occur in the IC. Nevertheless, about half of the IC has a PR reflectivity below 20 dBZ, indicating very light rain rates of approximately 1 mm hour^{-1} or less. About one-sixth of the included PR pixels have zero rain but are included when downgrading the resolution to match the TMI. The IC coverage of >20 dBZ reflectivity increases gradually with intensity, whereas the >30 and >40 dBZ coverage increases significantly for stronger storms. For 30 dBZ, coverage increases from 24% to 41% between TD and cat 3−5 ICs. Coverage of reflectivity above 40 dBZ rises from 4% in TDs to 12% in cat. 3−5 hurricanes. The coverage for cat. 1/2 hurricanes is more separated from TSs than it is for 85 GHz PCT <225 and <250 K. The IB and OB both have modest decreases in reflectivity coverage. The OB is the most uniform between intensity categories. The PR 2A25 rain rate can also be correlated with the coverage of PR reflectivity greater than 20, 30, and 40 dBZ, as displayed in Figure 8. The correlation coefficient is always highest for the 40 dBZ category, not a surprising result insofar as heavy rain contributes most to the mean rain rates. Correlations for >40 dBZ are always between 0.8 and 0.9, regardless of intensity. For the lower-reflectivity categories, the spread increases and the correlation coefficients drop. The 20 dBZ coverage does correlate fairly well with mean rain rate in the OB, but, in the inner regions, the higher prevalence of >30 dBZ echoes becomes the dominant signal.

4.3. Relating Convective Parameters to Algorithm Differences

[30] To examine whether the difference between the PR 2A25 and the TMI 2A12 rain estimates can be given as a function of convective parameters, correlation coefficients are calculated between the difference of the PR 2A25 and TMI 2A12 rain estimates and the percentage coverage of 37 and 85 GHz PCT less than certain values or PR reflectivity greater than certain values. Not surprisingly, the percentage coverage of 37 and 85 GHz PCT is not strongly related to the difference in rain rates. The storm regions that have a large difference in rain rate have a highly variable coverage of the various PCT parameters, and there is no evidence that the 37/85 GHz channels provide any additional insight to improve the TMI rain retrieval. Conversely, the coverage of PR reflectivity is more closely related to the rain rate difference, especially 40 dBZ, as pictured in the scatterplots in Figure 9. A distinctive linear relationship exists between the difference in rain rate and the percentage coverage of PR reflectivity >40 dBZ. Correlations are highest in hurricane ICs and IBs (≥0.80), whereas the OB region has much lower correlations. The large difference in the algorithms is caused mostly by the TMI significantly underestimating these areas of heavy rain. Weaker storms do not have as strong a relationship between algorithm differences and heavy rain

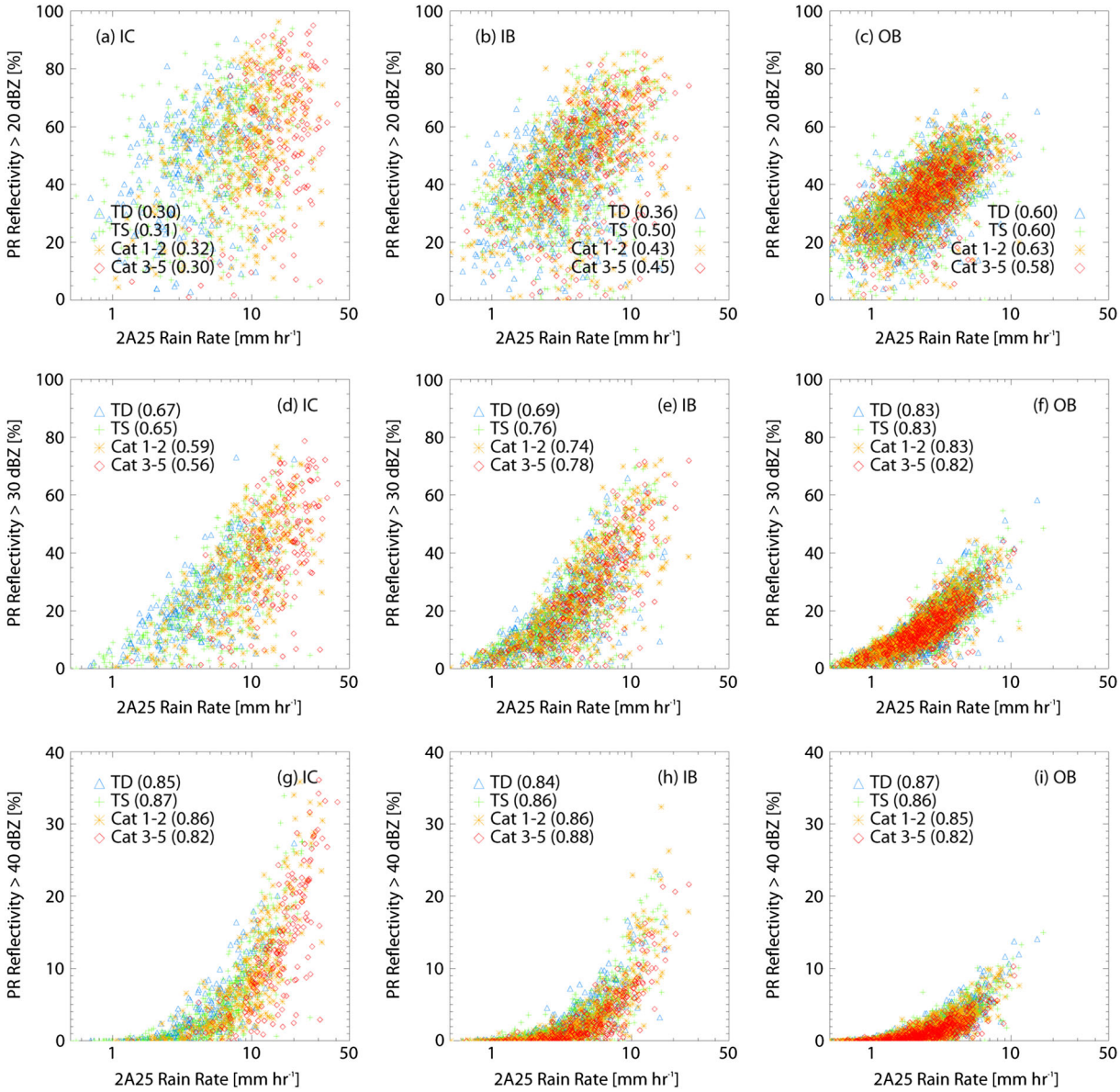

Figure 8. Scatterplots of PR 2A25 rain rate vs. percentage coverage of PR reflectivity >20, >30, and >40 dBZ. Plots are divided by IC, IB, and OB storm regions.

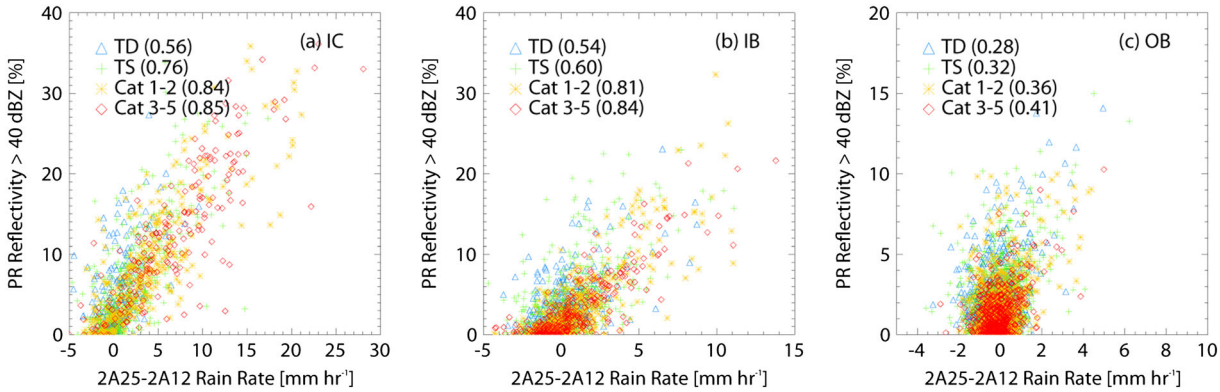

Figure 9. Scatterplots of the difference in PR and TMI rain rate (2A25 minus 2A12) vs. percentage coverage of PR reflectivity >40 dBZ for IC (a), IB (b), and OB (c) regions.

because most have only a small percentage (<10%) of rain with a PR reflectivity higher than 40 dBZ.

5. Discussion and Conclusions

[31] Using the TCPF database, TRMM overpasses of TCs over ocean are divided into the IC, IB, and OB regions. Rainfall and convective parameters are then calculated for each region. Emphasis is placed on comparing conditional rain rates because they are a direct estimate that does not depend on the orbital coverage. The PR 2A25 produces larger mean rain rates than the TMI 2A12 in the IC and IBs, with the difference always increasing with greater storm intensity. In hurricane ICs, the PR 2A25 mean rain rate is nearly double the TMI 2A12 mean rain rate. In the OBs, the algorithms show good agreement on rain rates, with the PR 2A25 measuring slightly higher rain rates than the TMI 2A12 in hurricanes and slightly lower rain rates than the TMI 2A12 in storms below hurricane strength. The OBs of tropical depressions are most similar to the ambient, non − TC-related tropical oceanic environment, which is known to have generally higher TMI 2A12 rain rates when averaged over monthly or annual time scales. In these outer rainband regions, the predominant source of disagreement is rainfall detection. The larger disagreements in inner areas are related to rainfall intensity.

[32] Because the TMI 2A12 has consistently larger raining areas, the volumetric rain (rain rate multiplied by raining area) is useful as an independent parameter to compare the total rainfall measured by the algorithms. The PR 2A25 volumetric rain is only greater than the TMI 2A12 in the inner regions (IC and IB) of cat. 3−5 hurricanes. In all storm regions, the TMI 2A12 volumetric rain exceeds the PR 2A25. The differences in volumetric rain arise because the greatest contribution to the mean rain rate comes from much higher maximum rain rates for the PR 2A25 compared with the TMI 2A12 [*Cecil and Wingo*, 2009]. The algorithms show the greatest disagreement when a large percentage of heavy rain is present, sometimes disagreeing by a mean rain rate of 20−30 mm hour^{-1} in hurricane ICs. The TMI 2A12 rarely detects rain rates above 15 mm hour^{-1}, but the PR 2A25 can reach 40−50 mm hour^{-1} averaged over some ICs because of its better sensitivity to high rain rates.

[33] Despite large differences in the mean rain rates of hurricane ICs, in 58% of ICs the algorithms are within 2 mm hour^{-1} of each other. Specifically, the difference between the algorithms (PR 2A25 minus TMI 2A12) is most closely correlated with the percentage coverage of PR reflectivity greater than 40 dBZ. The large difference in the algorithms is caused mostly by the TMI significantly underestimating moderate to heavy rain. In the IC, the TMI 2A12 rain rate retrievals are more closely correlated with the area of 85 GHz PCT <225 K (relative to raining area). In the IB and OB, the rain rate correlates best with the area of 85 GHz PCT <250 K. The TMI 2A12 rain rate also correlates well with the aerial coverage of 37 GHz PCT <275 K, especially in OBs and weaker storms. These convective parameters are good predictors of the mean TMI 2A12 rain rate, but they are poor indicators of the high PR 2A25 rain rates that cause the largest differences between the algorithms. Significant ice scattering is not a strong indicator that a TC will have high mean rain rates.

[34] It is necessary to consider the 85 GHz channel in order to achieve high-resolution rainfall retrievals. The downside is that the 85 GHz PCT is not an effective estimator of rain rates above about 15 mm hour^{-1}. Higher rain rates are detectable when a deep convective burst creates strong ice scattering, but other uncertainties remain, such as upper-level winds displacing the ice-scattering downshear of the low-level rain. Strong ice scattering (85 GHz PCT <225 K) is sometime isolated and is not always present in heavy rain. Large areas of heavy precipitation are common in the IC and IB regions, often without enough ice scattering above the precipitation to depress the brightness temperature significantly. The ice scattering can also look about the same, but with only light precipitation below. In OBs, heavy rain is usually both isolated and associated with strong 85 GHz ice scattering. As a result, the TMI 2A12 and PR 2A25 agree better when estimating OB rain rates, although the beam-filling effect may be responsible for TMI 2A12 underestimation in some cases.

[35] Based on these results, several possibilities for improving the TMI 2A12 algorithm appear promising. The latest version of the TMI 2A12 algorithm (version 7) includes the addition of PR vertical profiles to the TMI Bayesian precipitation profiles, which appears to reduce uncertainties in the TMI brightness temperate–rain rate relationship and improve the detection of moderate rain in the 15−25 mm hour^{-1} range. The PR is especially useful for identifying the regions where the TMI 2A12 is most significantly underestimating rain rates. Another option to consider is lowering the TMI 2A12 resolution to the 37 GHz or 19 GHz footprint. In TC rainfall, the 37 GHz channel is most sensitive in the 260-270 K range, although the combination of emission and scattering from both rain and ice hydrometers makes quantitative interpretation challenging. The relationship between the 37 GHz channel and rain rates is being investigated in more detail. Lowering the resolution below the 19 GHz footprint size prevents the rainbands from being adequately resolved. Finally, it may be advantageous to consider TCs as a separate regime with a modified TMI algorithm.

[36] This study highlights several important issues pertaining to the use of TMI 2A12 V6 in TCs. Previous studies that use the TMI 2A12 algorithm to quantify the mean spatial distribution of precipitation [e.g., *Lonfat et al*., 2004; *Chen et al*., 2006] likely underestimate the rainfall in the inner 100−200 km of hurricanes. Because the areas of heaviest rain are localized, it is likely that asymmetric TCs have a higher percentage of their rainfall in the favored quadrants than what is inferred with the TMI 2A12. Over 14 years of PR data are now available, so some aspects of these studies will be reconsidered using the PR 2A25 algorithm instead. The TMI 2A12 also fails to capture the high storm-to-storm variability of mean IC rainfall in hurricanes, as indicated in Figure 4a. For the TMI 2A12 to be applied to a small or localized set of case studies, it must be able to resolve better the unique properties of each individual storm, especially in extreme precipitation events. Computing the magnitude and extent of the heaviest precipitation areas is of utmost importance for determining the location and strength of a TC's inner regions and for assessing the flood potential as a storm approaches landfall. Continued improvement of the TMI

2A12 algorithm will allow for passive sensors to be more effectively utilized for these applications.

[37] **Acknowledgments.** The authors acknowledge Dr. Chris Kummerow for beneficial discussions about the TMI 2A12 algorithm. The authors thank three anonymous reviewers for useful comments, which helped to improve the manuscript substantially. The first author received support from a NASA Earth and Space Science Fellowship (NESSF) award (NNX11AP84H), and the second author received support from a NASA New Investigator Program (NIP) award (NNX10AG55G). Support for this study was also provided by the NASA Precipitation Measurement Mission (PMM) grant (NNX10AE28G) and NASA Hurricane Science Research Program (HSRP) grant (NNX10AG34G). The authors thank Drs. Ramesh Kakar and Ming-Ying Wei (NASA headquarters) for their continued support of TRMM/PMM and hurricane sciences and early career researchers in the field.

References

Berg, W., C. Kummerow, and C. A. Morales (2002), Differences between East and West Pacific rainfall systems, *J. Clim.*, *15*, 3659–3672, doi:10.1175/1520-0442(2002)015<3659:DBEAWP>2.0.CO;2.

Berg, W., T. L'Ecuyer, and C. Kummerow (2006), Rainfall climate regimes: The relationship of regional TRMM rainfall biases to the environment, *J. Appl. Meteorol. Climatol.*, *45*, 434–454, doi:10.1175/JAM2331.1.

Cecil, D. J. (2007), Satellite-derived rain rates in vertically sheared tropical cyclones, *Geophys. Res. Lett.*, *34*, L02811, doi:10.1029/2006GL027942.

Cecil, D. J., and M. Wingo (2009), Comparison of TRMM rain-rate retrievals in tropical cyclones, *J. Meteorol. Soc. Jpn.*, *87A*, 369−380, doi:10.2151/JMSJ.87A.369.

Cecil, D. J., and E. J. Zipser (1999), Relationships between tropical cyclone intensity and satellite-based indicators of inner core convection: 85-GHz ice-scattering signature and lightning, *Mon. Weather Rev.*, *127*, 103–123, doi:10.1175/1520-0493(1999)127<0103:RBTCIA>2.0.CO;2.

Cecil, D. J., E. J. Zipser, and S. W. Nesbitt (2002), Reflectivity, ice scattering, and lightning characteristics of hurricane eyewalls and rainbands. Part I: Quantitative description, *Mon. Weather Rev.*, *130*, 769–784, doi:10.1175/1520-0493(2002)130<0769:RISALC>2.0.CO;2.

Chen, S. S., J. A. Knaff, and F. D. Marks (2006), Effects of vertical wind shear and storm motion on tropical cyclone rainfall asymmetries deduced from TRMM, *Mon. Weather Rev.*, *134*, 3190–3208, doi:10.1175/MWR3245.1.

Iguchi, T., T. Kozu, R. Meneghini, J. Awaka, and K. Okamoto (2000), Rain-profiling algorithm for the TRMM Precipitation Radar, *J. Appl. Meteorol.*, *39*, 2038–2052, doi:10.1016/S0273-1177(99)00933-3.

Jiang, H., C. Liu, and E. J. Zipser (2011), A TRMM-based tropical cyclone cloud and precipitation feature database, *J. Appl. Meteorol. Climatol.*, *50*, 1255–1274, doi:10.1175/2011JAMC2662.1.

Jiang, H., E. M. Ramirez, and D. J. Cecil (2012), Convective and rainfall properties of tropical cyclone inner cores and rainbands from 11 years of TRMM data, *Mon. Weather Rev.*, doi:10.1175/MWR-D-11-00360.1.

Kummerow, C., W. S. Olson, and L. Giglio (1996), A simplified scheme for obtaining precipitation and vertical hydrometeor profiles from passive microwave sensors, *IEEE Trans. Geosci. Remote Sens.*, *34*, 1213−1232, doi:10.1109/36.536538.

Kummerow, C., W. Barnes, T. Kozu, J. Shiue, and J. Simpson (1998), The Tropical Rainfall Measuring Mission (TRMM) sensor package, *J. Atmos. Oceanic Technol.*, *15*, 809–817, doi:10.1175/1520-0426(1998)015<0809:TTRMMT>2.0.CO;2.

Kummerow, C., Y. Hong, W. S. Olson, S. Yang, R. F. Adler, J. McCollum, R. Ferraro, G. Petty, D.-B. Shin, and T. T. Wilheit (2001), The evolution of the Goddard Profiling Algorithm (GPROF) for rainfall estimation from passive microwave sensors, *J. Appl. Meteorol.*, *40*, 1801−1820, doi:10.1175/1520-0450(2001)040<1801:TEOTGP>2.0.CO;2.

Liu, C., E. J. Zipser, D. J. Cecil, S. W. Nesbitt, and S. Sherwood (2008), A cloud and precipitation feature database from nine years of TRMM observations, *J. Appl. Meteorol. Climatol.*, *47*, 2712–2728, doi:http://dx.doi.org/10.1175/2008JAMC1890.1.

Lonfat, M., F. D. Marks, and S. S. Chen (2004), Precipitation distribution in tropical cyclones using the Tropical Rainfall Measuring Mission (TRMM) microwave imager: A global perspective, *Mon. Weather Rev.*, *132*, 1645–1660, doi:10.1175/1520-0493(2004)132<1645:PDITCU>2.0.CO;2.

Mohr, K. I., and E. J. Zipser (1996), Mesoscale convective systems defined by their 85-GHz ice scattering signature: Size and intensity comparison over tropical oceans and continents, *Mon. Weather Rev.*, *124*, 2417–2437, doi:http://dx.doi.org/10.1175/1520-0493(1996)124<2417:MCSDBT>2.0.CO;2.

Molinari, J., P. Moore, and V. Idone (1999), Convective structure of hurricanes as revealed by lightning locations, *Mon. Weather Rev.*, *127*, 520-534, doi:10.1175/1520-0493(1999)127<0520:CSOHAR>2.0.CO;2.

Nesbitt, S. W., E. J. Zipser, and D. J. Cecil (2000), A census of precipitation features in the tropics using TRMM: Radar, ice scattering, and lightning observations, *J. Clim.*, *13*, 4087−4106, doi:10.1175/1520-0442(2000)013<4087:ACOPFI>2.0.CO;2.

Nesbitt, S. W., E. J. Zipser, and C. D. Kummerow (2004), An examination of Version-5 rainfall estimates from the TRMM microwave imager, precipitation radar, and rain gauges on global, regional, and storm scales, *J. Appl. Meteorol.*, *43*, 1016–1036, doi:10.1175/1520-0450(2004)043<1016:AEOVRE>2.0.CO;2.

Schumacher, C., and R. A. Houze (2000), Comparison of radar data from the TRMM satellite and Kwajalein Oceanic Validation Site, *J. Appl. Meteorol.*, *39*, 2151−2164, doi:10.1175/1520-0450(2001)040<2151:CORDFT>2.0.CO;2.

Shige, S., H. Sasaki, K. Okamoto, and T. Iguchi (2006), Validation of rainfall estimates from the TRMM precipitation radar and microwave imager using a radiative transfer model: 1. Comparison of the version-5 and -6 products, *Geophys. Res. Lett.*, *33*, L13803, doi:10.1029/2006GL026350.

Spencer, R. W., H. M. Goodman, and R. E. Hood (1989), Precipitation retrieval over land and ocean with the SSM/I: Identification and characteristics of the scattering signal, *J. Atmos. Oceanic Technol.*, *6*, 254−273, doi:10.1175/1520-0426(1989)006<0254:PROLAO>2.0.CO;2.

Wolff, D. B., and B. L. Fisher (2008), Comparisons of instantaneous TRMM ground validation and satellite rain-rate estimates at different spatial scales, *J. Appl. Meteorol. Climatol.*, *47*, 2215−2237, doi:10.1175/2008JAMC1875.1.